Sustainable Chemistry for the Environment 4 (2023) 100038

Contents lists available at ScienceDirect

Sustainable Chemistry for the Environment

journal homepage: www.sciencedirect.com/journal/sustainable-chemistry-for-the-environment

# Sunlight-driven photocatalytic degradation of Norfloxacin antibiotic in wastewater by ZnSe microsphere functionalized RGO composite

Suvendu Ghosh [a], Sayani Kar [a], Tanusri Pal [b,*], Surajit Ghosh [a,*]

[a] Department of Physics, Vidyasagar University, Midnapore, 721102 WB, India
[b] Department of Physics, Midnapore College, Midnapore 721101 WB, India

ARTICLE INFO

*Keywords:*
Norfloxacin antibiotic degradation
Photocatalysis
Reduced graphene oxide - semiconductor composite
Reactive species

ABSTRACT

The release of hazardous pollutants into the water, such as dyes, phenolic compounds, pesticides, different heavy metals, and antibiotics is the primary cause of environmental pollution. The solar energy-based photocatalysis technique has the potential to eliminate pollutants from the aquatic environment. ZnSe is a significant and commendable II-VI group photocatalyst having 2.82 eV direct band gap energy. Its performance towards degrading antibiotics in the presence of light was improved by anchoring it on the Reduced graphene oxide (RGO) matrix. Solution-processable RGO-ZnSe composites were characterized by X-ray diffraction, scanning electron microscopy, and transmission electron microscopy. Several spectroscopic studies like Raman spectroscopy, ultraviolet-visible spectroscopy, and photoluminescence spectroscopy were employed to illustrate the optical properties of the composites. The findings demonstrate that the ZnSe microsphere was supported effectively onto the two-dimensional RGO matrix. The performance of as-synthesized RGO-ZnSe composites was assessed based on the photocatalytic degradation of the antibiotic Norfloxacin in the presence of simulated solar light. An optimized RGO-ZnSe composite degrades approximately 83.5% of Norfloxacin in 40 min, while controlled-ZnSe photocatalysis only yields 33% in an identical experimental condition. The optimized RGO-ZnSe achieves the highest degradation reaction rate constant (k) of Norfloxacin ($k = 0.057\ min^{-1}$), and the k value is 4.38 times greater compared to the controlled-ZnSe microsphere. The light-dependent catalytic degradation mechanism was examined by employing scavenger experiments which gave away the responsible reactive radicals. Our results establish that the photo-generated hole has the leading role in the degradation of Norfloxacin in our system. In addition to that, the oxide radical and hydroxyl radical has also an important role in the degradation of Norfloxacin under our experimental condition. The finding suggests that the addition of RGO has enhanced photocatalytic performance and cyclic stability by preventing photo-generated electron-hole pair recombination. The photocatalytic oxidative deactivation mechanism of the Norfloxacin antibiotic was proposed. Our study offers new perceptiveness for the design of efficient solution-processable solar light-responsible photocatalysts for environmental pollution remediation.

## Introduction

Over the past few decades, antibiotics have been used as elixirs to protect humans and animals from various pathogens. The emanation of antibiotics from hospitals and farms is increasingly harmful to the aquatic environment. As a result, antibiotic concentrations in surface water [1], wastewater [2], and drinking water [3] have exceeded the permissible standards with the rapid development of medical science, agriculture, and animal farming [4]. A recent report reveals the existence of the residues of antibiotics in four Indian rivers' water [5]. This is of great concern to the scientist, as it will affect the problem of antimicrobial resistance. Among them, a substantial appearance of different antibiotics, like Norfloxacin, Ofloxacin, and Sulfamethoxazole, in the river water has been reported. Norfloxacin is considered a broad-spectrum fluoroquinolone antibiotic, extensively used to treat most gram-positive and gram-negative bacterial infections in many different parts of the body for humans and animals. The ubiquitous and rising concentration of Norfloxacin in water bodies may persuade the occurrence of microbial pathogens with antibiotic resistance, as a result, the existing antibiotic treatment becomes useless.

* Corresponding authors.
*E-mail addresses:* tanusripal@midnaporecollege.ac.in (T. Pal), surajit@mail.vidyasagar.ac.in (S. Ghosh).

https://doi.org/10.1016/j.scenv.2023.100038
Received 27 March 2023; Received in revised form 15 September 2023; Accepted 15 September 2023
Available online 16 September 2023

On the other hand, due to its poor metabolism, Norfloxacin molecules are accumulated widely in the aquatic environment, which has serious effects on general health and destroys the ecosystem balance [6]. Therefore, it is urgently required to find out a competent, environmentally beneficial method for the extensive elimination or deactivation of antibiotics from the environment, especially water bodies.

To remove antibiotics from the aquatic environment, many traditional physical and chemical schemes, like microbial degradation process [7], electrochemical techniques [8,9], physical adsorption [10–12], or advanced oxidation process (AOPs), like Fenton process [13], ozonation [14,15] have been employed. Owing to the stability and less biodegradability of the quinolone ring present in Norfloxacin, traditional methods are unable to reach the effective degradation of Norfloxacin. Besides, photocatalysis is considered the most efficient and eco-friendly approach to getting rid of antibiotics in the water body. Solar-light-responsive photocatalysis is also a cost-effective strategy as sunlight is an abundant source of energy.

Due to its tunable optoelectronic properties, enhanced light-induced charge-carrier separation, and altered surface photoactivity, ZnSe has been considered a potential and promising photocatalyst [16–19]. These excellent properties enable ZnSe to be used in organic contaminants purification [16], water splitting [17], $CO_2$ photo-reduction [18], and fuel cells [19]. But the structural instability, high electron-hole recombination probability, and less visible light absorption capability restrict the photocatalytic performance of ZnSe. The latest research establishes that making composite with 2D-graphene, reduced graphene oxide (RGO) or other carbon-based materials is an excellent way to resolve the problem and enhance the photocatalytic performance of semiconducting nanomaterials. Here the 2D material plays a dual role by dissociation of exciton at the interface and suppressing the recombination probability by providing a continuous pathway for the quick transportation of dissociated electrons [20–23]. Different RGO-based composite photocatalysts have successfully been exploited for the elimination of different organic water pollutants [24–28].

Recently few RGO-based composites have been utilized for the photocatalytic degradation of Norfloxacin antibiotic in aqueous environment. The photocatalytic degradation of Norfloxacin antibiotics using $FeNbO_4$-RGO nanocomposite was reported by Jones *et. al* [29]. Visible light-driven photocatalytic norfloxacin degradation in an aqueous medium by rGO/$Bi_2WO_6$ composite was reported by Zhao *et. al* [30]. Mohan *et. al* reported the visible-light photocatalytic norfloxacin degradation by reduced graphene oxide-coupled MnON nanospheres [31]. The photocatalytic degradation of norfloxacin by Tungsten/copper/cobalt atom oxide anchored $BiVO_4$-rGO has been reported by Selvakumar *et. al* [32]. Wang et al. described the simple synthesis of $AgVO_3$-rGO-$BiVO_4$ hetero junction for effective Norfloxacin detoxification and degradation under visible light illumination. [33].

Herein, we report the sunlight-driven degradation of Norfloxacin antibiotic using RGO-ZnSe composite photocatalyst synthesized by a solution process method. Here, the one-pot solvothermal route, which is considered a quick, economical, and successful approach was employed for the synthesis of the catalysts. As-synthesized composite photocatalyst was characterized structurally and optically. The performance of different responsive species that are accountable for the removal or deactivation of Norfloxacin antibiotics in a water medium has also been investigated. As per our knowledge, this is the first report on the photocatalytic Norfloxacin degradation by RGO-ZnSe composite. Our study establishes RGO-ZnSe as a potential catalyst for the efficient removal of Norfloxacin from the wastewater in the presence of light, which therefore significantly promotes the photocatalytic oxidation process.

## Experimental section

### *Materials*

Sigma Aldrich makes chemicals and reagents like Graphite powder, potassium persulfate, sodium nitrate, Polyvinylpyrrolidone (PVP), and phosphorus pentoxide were used here. Zinc acetate dihydrate and sodium selenite are both of them are Sigma Aldrich makes and are used as sources of zinc and selenium, respectively. Different acids, reducing agents, and solvents like hydrochloric acid [HCl], Sulfuric acid [$H_2SO_4$], hydrogen peroxide [$H_2O_2$], potassium permanganate [$KMnO_4$], ethylene diamine [$C_2H_8N_2$; ED], ethylene glycol [$C_2H_6O_2$; EG], ethylene diamine tetra acetate disodium (EDTA-$Na_2$), isopropyl alcohol (IPA), and hydrochloric acid [HCl], employed here were bought from Merck.

### *Synthesis of photocatalysts*

Graphene oxide (GO) was synthesized by the oxidation of graphite powder using Modified Hummers' method [34]. The composite of RGO-ZnSe was synthesized by a solution process method. Here, a one-pot, mono-step quick-to-achieve, and economical solvothermal process was adopted. Formation of RGO by reduction of GO, ZnSe microsphere from its precursor, and the attachment of the same onto the RGO mat were done at the same time. Here, 40 mg of GO was added to a glass beaker containing 25 ml mixed solvent of ED and EG (ED: EG = 1:24) at room temperature and sonicated for 10 min and thus a homogeneous solution was obtained. Then, 0.4 gm of PVP, 0.5 mmol of sodium selenite, and 0.5 mmol of Zinc acetate dihydrate were poured into the glass beaker of a mixed solution under continuous stirring magnetically. A homogenous mixture was formed after 30 min of stirring. A hydrothermal autoclave made up of a high-quality stainless-steel jacket with an inner Teflon chamber was used as a reactor. The homogenous mixture was then shifted to the reactor and then kept in a furnace for 12 h at 180 °C. Subsequently, the autoclave was gradually brought down to ambient temperature. A dark precipitate of RGO-ZnSe was collected and centrifuged (speed 8000 rpm) for 5 min. The synthesized materials were cleaned successively by the double distilled (DW) water several times to remove any impurities. Finally, as synthesized RGO-ZnSe composite was dried in a vacuum furnace for 5 h by annealing at 80 °C and named as RGO-ZnSe. The RGO was synthesized following the identical condition instead of the addition of $Zn(CH_3COO)_2$, PVP, and $Na_2SeO_3$ whereas, the controlled-ZnSe was synthesized without the addition of GO keeping unchanged the other experimental condition. A series of composites 20RGO-ZnSe, 30RGO-ZnSe, 50RGO-ZnSe, and 60RGO-ZnSe were synthesized by changing the amount of GO and keeping the amount of PVP, $Zn(CH_3COO)_2$, 2 $H_2O$ and $Na_2SeO_3$ unaltered. The synthesis process is schematically presented as Scheme 1.

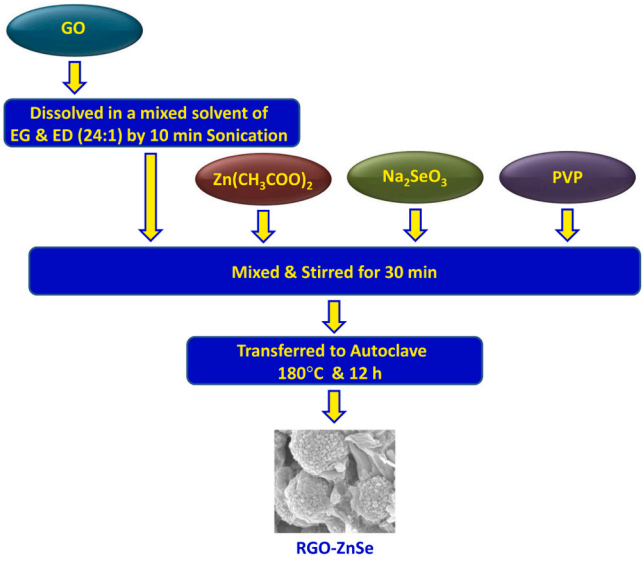


**Scheme 1.** Step wise representation of the RGO-ZnSe composite synthesis.

*Characterizations of photocatalysts*

Powder X-ray diffraction (PXRD) was performed by an X-ray diffractometer (Model: Rigaku-Miniflex, worked at the operating voltage and current as 40 kV and 10 mA) with Cu-$K_\alpha$ radiation having wavelength $\lambda = 0.15418$ nanometer. The data was collected for 2θ angles between 5° and 60° with a step size of 0.02°. The morphological study was executed by a scanning electron microscope (SEM; Zeiss Merlin). The micromorphology of the samples was imaged through a transmission electron microscope (TEM) and high-resolution TEM (HRTEM) (Model: JEOL-JEM 2100 F electron microscope) operating at 200 kV. Room temperature Raman spectra of GO and RGO-ZnSe composite were noted with a Renishaw, inVia Raman Microscope fitted with a 532 nm laser excitation. The absorption spectroscopy in the UV – Vis range was employed by a spectrophotometer (Agilent Cary Series). Room temperature photoluminescence (PL) studies were recorded by using a Perkin Elmer spectrofluorometer (Model LS – 55).

*Photocatalytic degradation experiments*

Photocatalytic assessments were carried out in a glass photoreactor which is placed in a beaker filled with cold water. A New Port Oreal Solar light simulator was employed as an illumination source for the catalytic reaction at room temperature. A Newport 843-R optical power meter was employed to measure the intensity of the illumination. To study the photocatalytic degradation, 20 mg of the photocatalyst was considered and dispersed in 20 ml of Norfloxacin (10 mg/L in water) solution under darkness. After attaining the adsorption-desorption equilibrium, the photo-reactor was illuminated under 100 mW $cm^{-2}$ simulated solar light for another 40 min. 5 ml of the solution was removed at 5 min intervals, then centrifugation was done to filter off photocatalysts. The absorption spectra of the degraded solution were recorded by the Spectrophotometer and the Norfloxacin concentration was assessed by studying the intensity variation of the characteristic peak of the absorption spectra. For the reusability test, the filter photocatalyst was recovered by centrifugation followed by heating at 100 °C to remove the surface organics.

## Results and discussion

*Materials characterization*

The PXRD pattern of graphite, GO, RGO, ZnSe, and RGO–ZnSe nanocomposite is presented in Fig. 1A. As illustrated in the figure, graphite and GO exhibit peaks at 2θ ≈ 26° and 10.4°, respectively. This broad peak of GO is attributed to the graphitic (002) plane having 0.85 nm d-spacing. The signature GO peak entirely vanished after the reduction of GO to RGO and a broad peak centered at 25.08° appears. The peaks of ZnSe are indexed to the planes of (111), (022), and (113) and it is in excellent accord with the cubic zinc blende (ZB) type crystal structure [35]. The inter-planner spacing and the inter-atomic distances of the controlled-ZnSe sample were calculated as 0.327 and 0.567 nm respectively, for the (111) lattice plane. No shifting of signature peaks of the ZnSe is found in the PXRD of the composite of RGO-ZnSe, which indicates the crystal structure of ZnSe is not tuned by the RGO. The distinct hump of RGO is absent in the PXRD profile of the as-synthesized composite as the crystallinity of ZnSe dominates over the crystallinity of RGO formed by the graphitic planes. The non-appearance of additional peaks in the XRD pattern of the RGO-ZnSe compound ruled out the creation of any other impurities during the chemical reaction. Fig. 1B demonstrates the RGO-ZnSe composite's SEM image, where the amalgamation of the ZnSe microsphere within RGO is observed. Each ZnSe microsphere is made by the self-assembly of nanoparticles, which results in the materialization of a 3-dimensional structure of ZnSe. The presence of wrinkles on the RGO sheet is also observed which is formed during the solvothermal reaction. The presence of wrinkles may increase the catalytic performance of the RGO-ZnSe compound [36]. The structural and microstructural information was acquired from the TEM and HRTEM images of the compound and is presented in Fig. 1C. The TEM image depicts the well-distributed attachment of ZnSe onto the wrinkled 2D RGO sheet. Here the RGO sheets facilitate the uniform distribution of ZnSe on its vast 2D canvas, as well as, prevent the aggregation of ZnSe efficiently. On the other hand, the wrinkled surface of RGO could provide a large contact interface between RGO and ZnSe. This close interfacial contact facilitates the photo-induced charge transfers from the ZnSe to RGO sheets. The lattice fringe distance was calculated as 0.33 nm from the HRTEM image of ZnSe (Inset of Fig. 1C). This spacing value is perfectly consistent with the result obtained from the PXRD pattern. The highly crystalline fringe visible in the HRTEM image could provide improved exciton diffusion length, consequently leading to enhance the generation of photocurrent and boosting the photocatalytic performance of the compound. The HRTEM image also ruled out the probability of core-shell formation of RGO and ZnSe.

Fig. 2A presents the Raman spectrum in the wavelength range of 1100 – 1700 $cm^{-1}$ of as-synthesized GO and the composite (RGO-ZnSe). Raman spectroscopy confirmed the GO reduction. The Raman spectra of GO display two vibrational bands centered at 1348 $cm^{-1}$ and 1593 $cm^{-1}$, ascribed to K-point phonons of $A_{1g}$ symmetry and zone-center phonons of $E_{2g}$ symmetry within the $sp^2$ bonded carbon atoms, respectively. A substantial gain in the D-band to G-band intensity ratio from 0.99 to 1.16 was observed in the composite, which authenticates the successful GO reduction and prepares RGO in the synthesized composite [37,38].

The optical absorption spectra of controlled-ZnSe and RGO-ZnSe

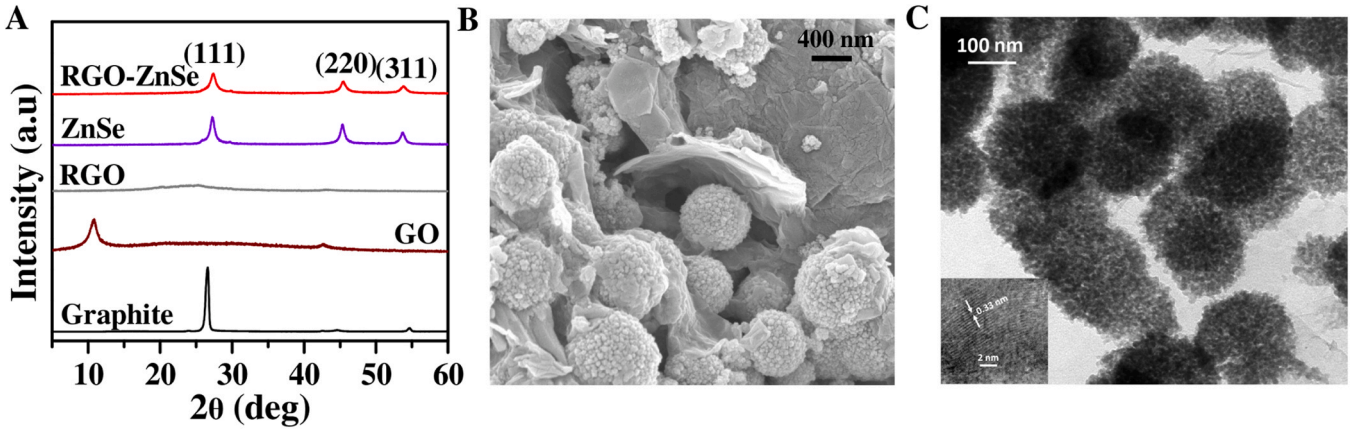


**Fig. 1.** (A) PXRD pattern of all the synthesized materials (B) SEM and (C) TEM image of RGO-ZnSe and the HRTEM of ZnSe on RGO (inset).

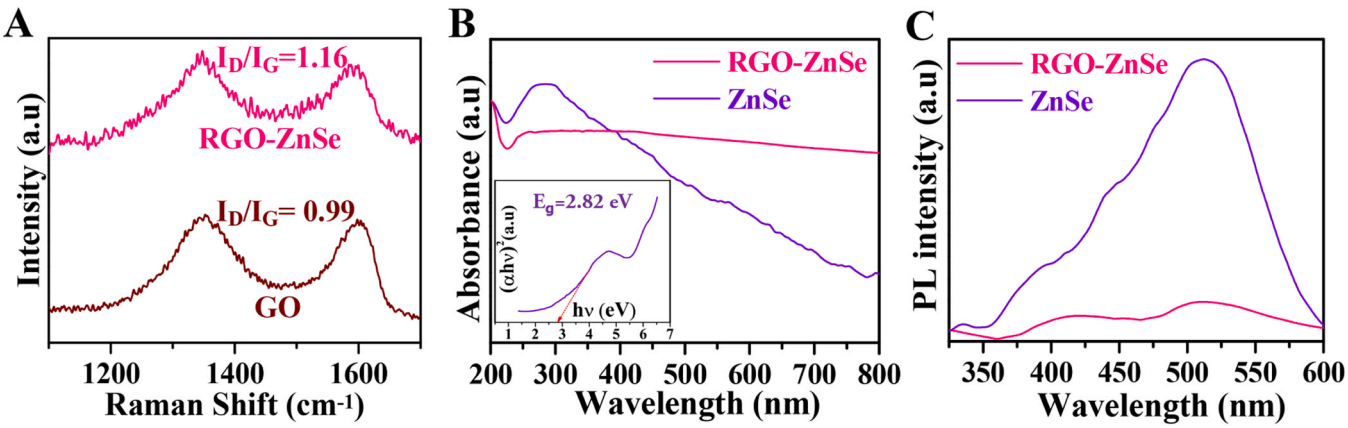


**Fig. 2.** (A) Raman spectra of GO and RGO composite. (B) Optical absorption and (C) Photoluminescence spectra of controlled-ZnSe and the RGO–ZnSe composite photocatalyst. $(\alpha h\nu)^2$ vs. hν for controlled-ZnSe in the inset of (B).

compounds were recorded from 200 nm to 800 nm and are presented in Fig. 2B. The optical bandgap ($E_g$) of ZnSe was estimated by analyzing the absorption spectra in the framework of Tauc's relation [39] as $(\alpha h\nu)^2 = A(h\nu - E_g)$, where $h\nu$ is the energy of the photon. The $E_g$ of controlled-ZnSe was estimated as 2.82 eV by plotting $(\alpha h\nu)^2 vs. h\nu$ graph [inset of Fig. 2B]. The edge of the optical spectra of the RGO-ZnSe compound looks moderately similar to controlled-ZnSe, which excludes the chances of RGO incorporation into the lattice site of ZnSe. Moreover, the RGO-ZnSe compound absorbs more light compared to controlled-ZnSe, which might be due to the reduction of reflection of light owing to the existence of RGO in the compound. Broadband absorption spectra starting from 250 to 800 nm of solution-processable RGO-ZnSe composite in the visible region establishes it as a promising candidate as a photocatalyst. The high absorbance capability with a broad absorbance range of optical photons and the efficient light-generated carrier formation are the two key factors of a material to be an efficient photocatalyst. To assess the photo-induced charge generation capability, the photoluminescence study of controlled -ZnSe and its composite with RGO was carried out at room temperature (excitation wavelength: 300 nm) and is presented in Fig. 2C. In photoluminescence spectra of controlled-ZnSe, a broad emission peak is observed centered at 510 nm, which might be due to the presence of interstitials and vacancies of Zn and/or Se atoms [40] which were completely quenched for RGO-ZnSe composite. The PL spectra of controlled-ZnSe depict the generation of charge carriers in controlled-ZnSe under illumination. Whereas, the quenching of PL spectra establishes the strong and effective interfacial charge transfer from ZnSe to RGO sheets [41]. The high absorption capacity in the UV-Vis region, with efficient photo-induced charge generation and effective interfacial photo-induced charge transfer, signifies the potentiality of RGO-ZnSe as an efficient composite photocatalyst for the effective elimination of aquatic pollutants.

*Sunlight-driven Norfloxacin degradation by the synthesized photocatalyst*

The solar light-induced photo-deactivation kinetics of the aqueous solution of Norfloxacin antibiotics was investigated by UV−Vis absorption study in the presence of different photocatalysts. Typically, in an aqueous solution of Norfloxacin, required amount of photocatalysts was added under the dark and stirred for 40 min. After reaching the adsorption equilibrium, the photocatalysis experiment was carried out for 40 min under the illumination of light. The absorption spectra of the Norfloxacin in the presence of the catalysts are presented in Fig. S1, of Supporting Information (SI). A small change in the concentration of Norfloxacin by RGO-ZnSe composite was observed in the darkness (Fig. S2A, of SI), which might be due to the adsorption of Norfloxacin at the surface of the catalyst. No considerable variation of Norfloxacin concentration was noticed in the nonappearance of the photocatalysts under 40 min of solar light illumination (Fig. S2B, of SI), which ruled out the self-photo-degradation of Norfloxacin within our experimental time frame. Fig. S1, of SI, depicts that the concentration of Norfloxacin decreases with the illumination time of the simulated solar radiation. The efficiency of Norfloxacin degradation was calculated by the relation [42, 43].

$$Degradation \quad Efficiency \quad (\%) = \left(1 - \frac{C}{C_0}\right) \times 100\%$$

Where, the initial concentration (t = 0) of Norfloxacin is $C_0$, and C is the concentration of it at a particular interval of time (here 5 min) under the illumination of light. Fig. 3A shows the degradation efficiency of ZnSe and RGO-ZnSe for different times of illumination. It is observed from the figure that RGO-ZnSe are efficiently able to degrade Norfloxacin and which is 83.5 ( ± 0.7) % in 40 min. Whereas, only 33% of Norfloxacin was degraded in the presence of controlled-ZnSe keeping identical measuring conditions. To understand the possible mechanism of Norfloxacin degradation, photodegradation kinetics was studied. Recent studies establish that the photocatalytic degradation kinetics of water pollutants follows the model of pseudo-first-order kinetics [44–47]:

$$Ln \quad \frac{C_0}{C} = kt$$

where k and t are the reaction rate constant and time, respectively. Fig. 3B compares the variation of $Ln\frac{C_0}{C}$ with t for all the catalysts. Both the curves follow the linear variation and the k value was determined from the linear fit. The values of k for both the catalysts and controlled-ZnSe are presented in the inset of Fig. 3B. As shown in figure, RGO-ZnSe poses a 4.38 times higher k value than controlled-ZnSe. To ensure reproducibility, we have carried out the experiments of adsorption, photolysis, as well as photocatalysis experiment for three additional batches of RGO-ZnSe photocatalyst were considered. No appreciable variation in the outcomes was found. The results of the reproducibility test are presented as Fig. S3, of SI.

According to the excitonic picture, a when ZnSe is irradiated by light excitons are generated, and free carriers are formed after dissociation of excitons at the defects state present in the ZnSe sample and most of the electron-hole recombines immediately. In contrast, in the RGO-ZnSe composite, the electrons move from ZnSe to RGO, leaving a hole in ZnSe. This reduces the electron-hole recombination possibilities and subsequently improves the photocatalytic performance of the composite.

To assess the loading effect of RGO on the photocatalytic action of RGO-ZnSe, a series of composites with different RGO loading were synthesized. Considering the present composite as RGO-ZnSe where

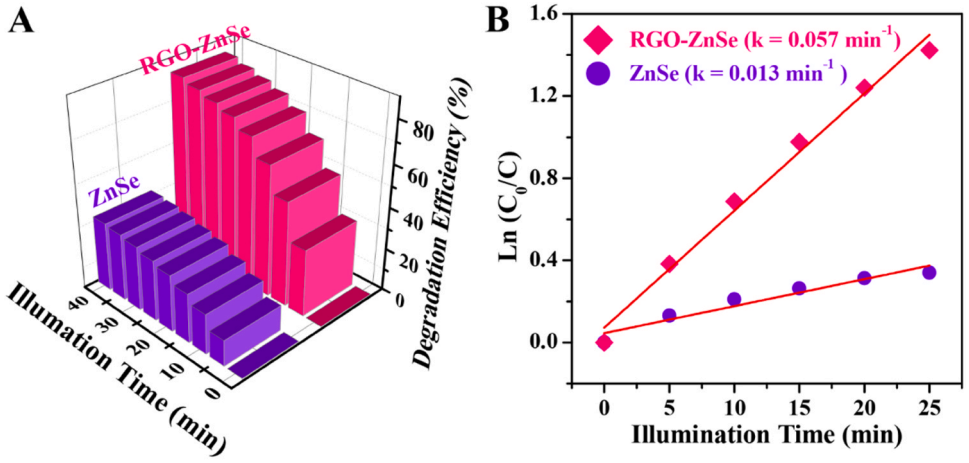


**Fig. 3.** (A) Degradation efficiency and (B) Kinetics of controlled-ZnSe and the RGO-ZnSe compound photocatalyst.

40 mg GO is used to form its composites. The photocatalytic activities of a series of catalysts with different amounts of GO (the source of RGO) like 20 mg (20RGO-ZnSe), 30 mg (30RGO-ZnSe), 50 mg (50RGO-ZnSe), and 60 mg (60RGO-ZnSe) were investigated in the same experimental circumstances. The visible light absorption spectra of Norfloxacin in an aqueous medium in the presence of different RGO-ZnSe catalysts are presented in Fig. S4, of SI.

Fig. 4A shows the comparison of the degradation efficiency of different RGO-ZnSe catalysts, where the highest value of degradation efficiency is observed for the 40RGO-ZnSe composite, which we marked as RGO-ZnSe here. The change in $Ln\frac{C_0}{C}$ with the illuminating period is presented in Fig. 4B. The k values which are evaluated from the linear fit of $Ln\frac{C_0}{C}$ vs t graph are presented in Fig. 4C. As shown in the figure, the highest degradation rate constant is shown by the RGO-ZnSe (40RGO-ZnSe) catalyst. In the RGO-ZnSe composite, the RGO mat serves as a platform for the attachment of the ZnSe nanosphere and assemble the electrons from the conduction band of ZnSe. In the composite, when the RGO quantity is less than 40, the amount of RGO is insufficient to provide enough surface to bind ZnSe. Therefore, the recombination probability of photo-generated electrons and holes is not modified by the RGO significantly. If the RGO content is increased by more than 40, there is a possibility that the extra RGO mat may cover the ZnSe nanospheres, reducing the amount of ZnSe that is exposed in the composite. As a result, less amount of excitons are formed subsequently the photocatalytic activity of the composite decreases.

In the photocatalytic process, the photo-generated charge carriers, different radicals like hydroxyl ($OH^{\bullet}$), and superoxide ($O_2^{\bullet-}$) are considered the vital reactive species accountable for the photocatalytic degradation of different organic water pollutants. To further expose the significant insight into the photocatalytic mechanism for the degradation of Norfloxacin antibiotic, and to explore the role of different responsive species on the degradation, different scavengers like, EDTA-$Na_2$, scavenger of the hole ($h^+$) [48]; nitrogen atmosphere, scavenger of $O_2^{\bullet-}$ radicals [49] and IPA, scavenger of $OH^{\bullet}$ radicals [50] were used. The optical absorption spectra of Norfloxacin in the presence of both the RGO-ZnSe catalysts and different quenching agents under solar illumination are presented in Fig. S5, of SI. Fig. 5 shows the variation of degradation efficiency (Fig. 5A), and $Ln\frac{C_0}{C}$ (Fig. 5B) with the time of illumination, and the k values (Fig. 5C) for different quenching agents for RGO-ZnSe photocatalyst. In the absence of any quenching agents, more than 83% of the Norfloxacin was degraded within 40 min. of solar light illumination, which declines to 71%, 61%, and 14% in the presence of IPA, $N_2$ atmosphere, and EDTA-$Na_2$ respectively under the identical environment. Remarkably low k value in the presence of EDTA-$Na_2$ depicts that photo-generated hole has the leading role in the degradation of Norfloxacin in our system. The reduction of degradation efficiency in the presence of an $N_2$ atmosphere and IPA proves that the oxide radical and hydroxyl radical has an important role in the degradation of Norfloxacin under our experimental condition. Based on the scavenger study we have tried to establish the mechanism of the formation of responsive species and degradation of Norfloxacin by RGO-ZnSe catalysts in the presence of solar light which is presented in Fig. 6. The

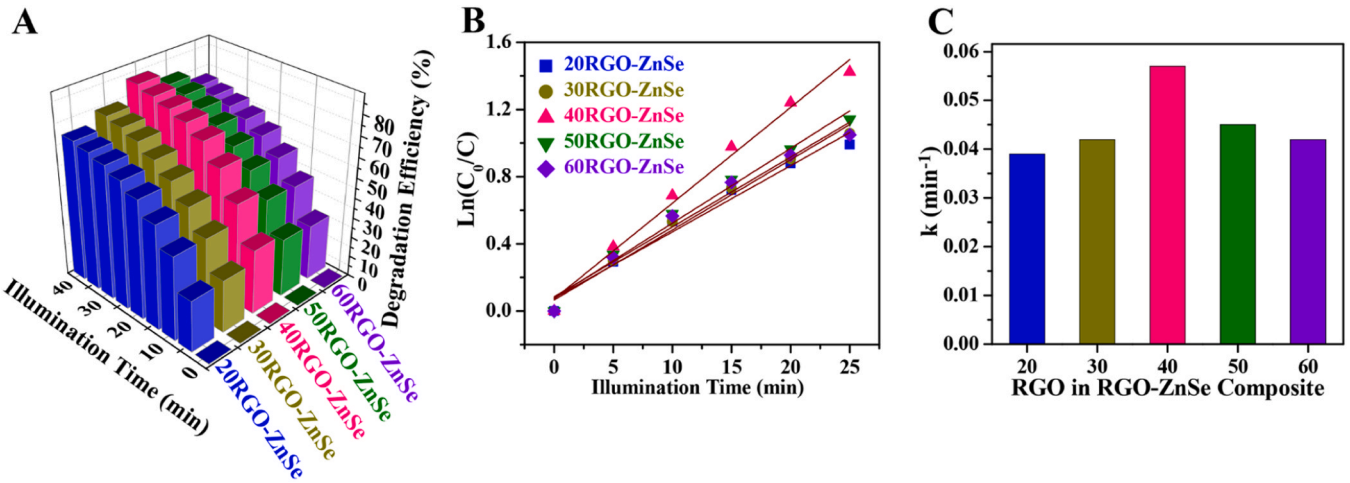


**Fig. 4.** (A) Degradation efficiency (B) Kinetics and (C) rate constant of RGO-ZnSe compound photocatalyst with different RGO loading.

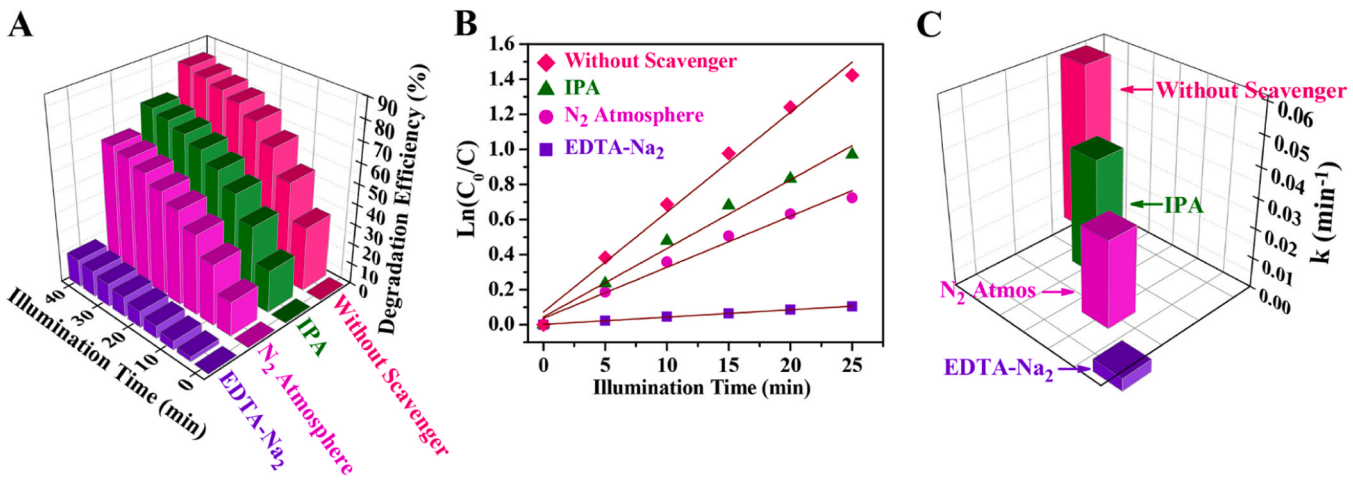


**Fig. 5.** (A) Degradation efficiency (B) Kinetics and (C) rate constant of RGO-ZnSe photocatalyst in presence of different scavengers.

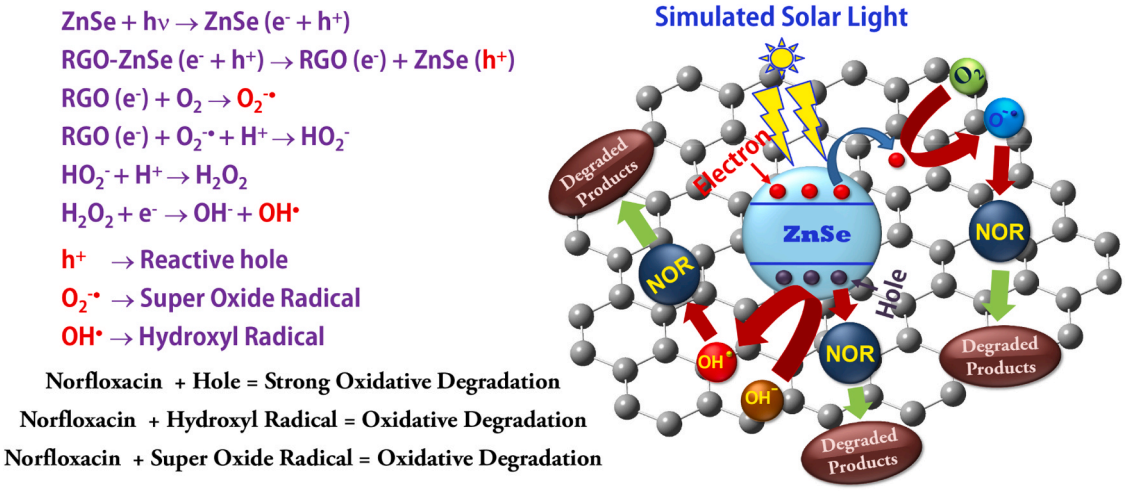


**Fig. 6.** Formation mechanism of $h^+$, $O_2^{\bullet}$ & $OH^{\bullet}$ radical and cartoon of photocatalytic degradation of Norfloxacin by RGO-ZnSe composite in presence of light.

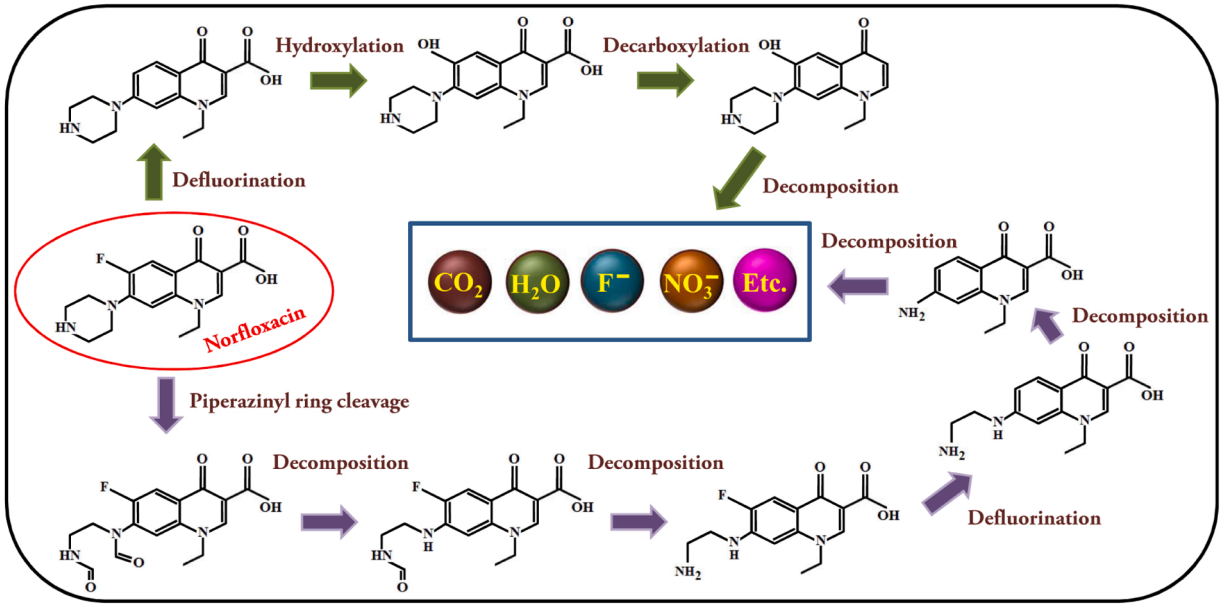


**Fig. 7.** Probable degradation pathways of Norfloxacin in this system.

oxidative deactivation of Norfloxacin is based on defluorination, decarboxylation, the demolition of the piperazinyl group, and a hydroxylation reaction [51]. The possible degradation pathway is presented in Fig. 7.

In addition to the high photodegradation efficiency, reusability, and stability are the figures of merit for a photocatalyst for its real-life applications. To examine the reusability of the RGO-ZnSe catalyst, five consecutive photo deactivation studies were carried out under identical experimental conditions where fresh Norfloxacin solution was used after each reaction cycle and the results are compared in Fig. S6A in SI. The photodegradation efficiency declines from 83.5% to 73% after five successive photodegradation cycles. This decrease in photodegradation efficiency may be ascribed to the adsorption of the residual Norfloxacin and intermediates on the exterior of the photocatalyst during the recycled studies and the loss of photocatalyst during the recycling use of the photocatalyst [52]. To check the structural firmness of the synthesized catalyst, XRD of RGO-ZnSe was carried out after five rounds of deactivation of Norfloxacin and is displayed in Fig. S6B. No noticeable change in the XRD pattern was observed, which authenticates the structural firmness of the RGO-ZnSe catalyst.

## Conclusion

Due to its suitable energy band positions, ZnSe, an intrinsic semiconductor (direct band material of $E_g = 2.82$ eV), has received favorable consideration for energy absorption and water decontamination. However, there are a few drawbacks, such as an unstable structure and a faster recombination rate, which limit the ZnSe performance. Anchoring ZnSe on the matrix of RGO improves photocatalytic performance in many folds. Herein, a series of RGO-ZnSe composite catalysts were synthesized and characterized in terms of their optical properties, chemical composition, surface morphology, and crystalline structure. The findings confirmed that the ZnSe microsphere was successfully anchored onto the surface of RGO. The degradation of the antibiotic Norfloxacin in the presence of light was employed to investigate the photocatalytic performance of the catalyst. The findings demonstrated that the RGO has a substantial influence on the photocatalytic activities of ZnSe. Adsorption and photocatalytic efficiency of the controlled-ZnSe microsphere improved in the composite formation as RGO played an important role by preventing the photogenerated $e^-$ and $h^+$ recombination probabilities. The solution processable RGO-ZnSe composite yielded 83.5% degradation of Norfloxacin in 40 min while controlled-ZnSe photocatalysis only yielded 33% in an identical experimental condition. The optimized RGO-ZnSe achieves the highest degradation reaction rate constant (k) of Norfloxacin ($k = 0.057$ min$^{-1}$) is 4.38 times greater than controlled-ZnSe ($k = 0.013$ min$^{-1}$). Further investigation revealed that the prime responsive species in the degradation of Norfloxacin in our system is the photo-generated hole. In addition to that, the oxide radical and hydroxyl radical have also performed a significant part in the degradation of Norfloxacin in our case. Accordingly, the mechanism of a photocatalytic reaction was proposed. The RGO-ZnSe composite appears to be an effective catalyst for eliminating antibiotics from wastewater. Our study offers novel information for designing high-performance solution processable solar photocatalysts for environmental pollution remediation.

## Declaration of Competing Interest

The authors declare that they have no known competing financial interests or personal relationships that could have appeared to influence the work reported in this paper.

## Data Availability

Data will be made available on request.

## Acknowledgments

This work was supported by the Council of Scientific & Industrial Research (CSIR), New Delhi, India via grant 03(1392)/16/EMR-II. We are also thankful to the Department of Science and Technology (DST) and University Grants Commission (UGC), New Delhi, India for providing infrastructural support and special assistance to the Department of Physics, Vidyasagar University, via FIST and SAP programs respectively.

## Appendix A. Supporting information

Supplementary data associated with this article can be found in the online version at doi:10.1016/j.scenv.2023.100038.

## References

[1] J.L. Wilkinson, et al., Pharmaceutical pollution of the world's rivers, 2113947119, PNAS 119 (2022), https://doi.org/10.1073/pnas.2113947119.
[2] K. He, L. Blaney, Systematic optimization of an SPE with HPLC-FLD method for fluoroquinolone detection in wastewater, J. Hazard. Mater. 282 (2015) 96–105, https://doi.org/10.1016/j.jhazmat.2014.08.027.
[3] Y. Wang, X. Dong, J. Zang, X. Zhao, F. Jiang, L. Jiang, C. Xiong, N. Wang, C. Fu, Antibiotic residues of drinking-water and its human exposure risk assessment in rural Eastern China, Water Res 236 (2023), 119940, https://doi.org/10.1016/j.watres.2023.119940.
[4] B. Luo, D. Xu, D. Li, G. Wu, M. Wu, W. Shi, M. Chen, Fabrication of a Ag/$Bi_3TaO_7$ plasmonic photocatalyst with enhanced photocatalytic activity for degradation of tetracycline, ACS Appl. Mater. Interfaces 7 (2015) 17061–17069, https://doi.org/10.1021/acsami.5b03535.
[5] Project report published by Toxics Link, 2022, Menace of antibiotic pollution in Indian rivers Supervised by: P. Mohapatra; Studied and Reported by: O. Gaonkar, T. Arora.
[6] X. –L. Zhao, P. Li, S. –Q. Zhang, S. –W. He, S. –Y. Xing, Z. –H. Cao, R. Lu, Z. –H. Li, Effects of environmental norfloxacin concentrations on the intestinal health and function of juvenile common carp and potential risk to humans, Environ. Pollut. 287 (2021), 117612, https://doi.org/10.1016/j.envpol.2021.117612.
[7] A. Kayal, S. Mandal, Microbial degradation of antibiotic: future possibility of mitigating antibiotic pollution, Environ. Monit. Assess. 194 (2022) 639, https://doi.org/10.1007/s10661-022-10314-2.
[8] Y. Kitazono, I. Ihara, G. Yoshida, K. Toyoda, K. Umetsu, Selective degradation of tetracycline antibiotics present in raw milk by electrochemical method, J. Hazard. Mater. 243 (2012) 112–116, https://doi.org/10.1016/j.jhazmat.2012.10.009.
[9] X. Peng, J. Cao, B. Xie, M. Duan, J. Zhao, Evaluation of degradation behavior over tetracycline hydrochloride by microbial electrochemical technology: performance, kinetics, and microbial communities, Ecotoxicol. Environ. Saf. 188 (2020), 109869, https://doi.org/10.1016/j.ecoenv.2019.109869.
[10] D. Mangla, Annu, A. Sharma, S. Ikram, Critical review on adsorptive removal of antibiotics: Present situation, challenges and future perspective, J. Hazard. Mater. 425 (2022), 127946, https://doi.org/10.1016/j.jhazmat.2021.127946.
[11] T. –H. Dao, T.-Q.-M. Vu, N.-T. Nguyen, T.-T. Pham, T.-L. Nguyen, S. Yusa, T. –D. Pham, Adsorption characteristics of synthesized polyelectrolytes onto alumina nanoparticles and their application in antibiotic removal, Langmuir 36 (2020) 13001–13011, https://doi.org/10.1021/acs.langmuir.0c02352.
[12] M.N. Alnajrani, O.A. Alsager, Removal of antibiotics from water by polymer of intrinsic microporosity: Isotherms, kinetics, thermodynamics, and adsorption mechanism, Sci. Rep. 10 (2020) 794, https://doi.org/10.1038/s41598-020-57616-4.
[13] M. Hassana, G.A. Ashraf, B. Zhang, Y. Hea, G. Shen, S. Hu, Energy-efficient degradation of antibiotics in microbial electro-Fenton system catalysed by M-type strontium hexa ferrite nanoparticles, Chem. Eng. J. 380 (2020), 122483, https://doi.org/10.1016/j.cej.2019.122483.
[14] S.N. Malik, P.C. Ghosh, A.N. Vaidya, S.N. Mudliar, Hybrid ozonation process for industrial wastewater treatment: principles and applications: A review, J. Water Process Eng. 35 (2020) 10119, https://doi.org/10.1016/j.jwpe.2020.101193.
[15] P. Li, R. Miao, P. Wang, F. Sun, X. Li, Bi-metal oxide-modified flat-sheet ceramic membranes for catalytic ozonation of organic pollutants in wastewater treatment, Chem. Eng. J. 426 (2021), 131263, https://doi.org/10.1016/j.cej.2021.131263.
[16] K. Feng, W. Huang, Z. Fu, X. Hu, J. Fan, E. Liu, Effective $H_2O_2$-Free photo-Fenton processes over ZnSe nanosheets for photocatalytic degradation of dyes and antibiotics, J. Taiwan Inst. Chem. Eng. 134 (2022), 104312, https://doi.org/10.1016/j.jtice.2022.104312.
[17] M.F. Kuehnel, C.E. Creissen, C.D. Sahm, D. Wielend, A. Schlosser, K.L. Orchard, E. Reisner, ZnSe nanorods as visible-light absorbers for photocatalytic and photoelectrochemical $H_2$ evolution in water, Angew. Chem. 131 (2019) 5113–5117, https://doi.org/10.1002/anie.201814265.
[18] Z.-K. Xin, M. –Y. Huang, Y. Wang, Y. –J. Gao, Q. Guo, X. –B. Li, C. –H. Tung, L. –Z. Wu, Reductive carbon–carbon coupling on metal sites regulates photocatalytic $CO_2$ reduction in water using ZnSe quantum dots, 202207222, Angew. Chem. Int. 61 (2022), https://doi.org/10.1002/anie.202207222.

[19] M. Prabhu, K. Kamalakkannan, N. Soundararajan, K. Ramachandran, Fabrication and characterization of ZnSe thin films based low-cost dye sensitized solar cells, J. Mater. Sci.: Mater. Electron. 26 (2015) 3963–3969, https://doi.org/10.1007/s10854-015-2931-5.

[20] K. Chakraborty, S. Chakrabarty, T. Pal, S. Ghosh, Synergistic effect of zinc selenide - reduced graphene oxide towards enhanced solar-light-responsive photo current generation and photocatalytic 4-nitrophenol degradation, N. J. Chem. 41 (2017) (2017) 4662–4671.

[21] T. Wang, D. Yue, X. Li, Y. Zhao, Lead-free double perovskite $Cs_2AgBiBr_6$/RGO composite for efficient visible light photocatalytic $H_2$ evolution, Appl. Catal. B Environ. 268 (2020), 118399, https://doi.org/10.1016/j.apcatb.2019.118399.

[22] P. Sharma, N. Kumar, R. Chauhan, V. Singh, V.C. Srivastava, R. Bhatnagar, Growth of hierarchical ZnO nano flower on large functionalized rGO sheet for superior photocatalytic mineralization of antibiotic, Chem. Eng. J. 392 (2020), 123746, https://doi.org/10.1016/j.cej.2019.123746.

[23] S.M. Ghoreishian, K.S. Ranjith, B. Park, S.-K. Hwang, R. Hosseini, R. Behjatmanesh-Ardakani, S.M. Pourmortazavi, H.U. Lee, B. Son, S. Mirsadeghi, Y. –K. Han, Y. S. Huh, Full-spectrum-responsive $Bi_2S_3$@CdS S-scheme hetero structure with intimated ultrathin RGO toward photocatalytic Cr(VI) reduction and $H_2O_2$, Chem. Eng. J. 419 (2021), 129530, https://doi.org/10.1016/j.cej.2021.129530.

[24] X. Liu, T. Xu, P. Wang, J. Cao, Y. Chen, H. Fan, X. Meng, M. Wei, H. Liu, L. Yang, Enhanced visible light photocatalytic activities of 3D Fe3O4@SiO2@ZnO/ ZnS nanocomposites by assembling 2D graphene sheets, Phys. E 134 (2021), 114926, https://doi.org/10.1016/j.physe.2021.114926.

[25] S. Kaushal, V. Kumari, P. Pal Singh, Sunlight-driven photocatalytic degradation of ciprofloxacin and organic dyes by biosynthesized rGO-$ZrO_2$ nanocomposites, Environ. Sci. Pollut. Res. Int 30 (2023) 65602–65617, https://doi.org/10.1007/s11356-023-27000-6.

[26] M. Athari, M. Fattahi, M. Khosravi-Nikou, A. Hajhariri, Adsorption of different anionic and cationic dyes by hybrid nanocomposites of carbon nanotube and graphene materials over UiO-66, Sci. Rep. 12 (2022) 20415, https://doi.org/10.1038/s41598-022-24891-2.

[27] H.A. Patehkhor, M. Fattahi, M. Khosravi-Nikou, Synthesis and characterization of ternary chitosan–$TiO_2$–ZnO over graphene for photocatalytic degradation of tetracycline from pharmaceutical wastewater, Sci. Rep. 11 (2021) 24177, https://doi.org/10.1038/s41598-021-03492-5.

[28] P. Ghasemipour, M. Fattahi, B. Rasekh, F. Yazdian, Developing the ternary ZnO doped $MoS_2$ nanostructures grafted on CNT and reduced graphene oxide (RGO) for photocatalytic degradation of aniline, Sci. Rep. 10 (2020) 4414, https://doi.org/10.1038/s41598-020-61367-7.

[29] B.M.F. Jones, D. Maruthamani, V. Muthuraj, Construction of novel n-type semiconductor anchor on 2D honey comb like $FeNbO_4$/RGO for visible light drive photocatalytic degradation of norfloxacin, J. Photochem. Photobiol. A 400 (2020), 112712, https://doi.org/10.1016/j.jphotochem.2020.112712.

[30] Y. Zhao, X. Liang, X. Hu, J. Fan, rGO/$Bi_2WO_6$ composite as a highly efficient and stable visible-light photocatalyst for norfloxacin degradation in aqueous environment, J. Colloid Interface Sci. 589 (2021) 336–346, https://doi.org/10.1016/j.jcis.2021.01.016.

[31] H. Mohan, S. Vadivel, P.M. Sathya, M. Fujii, G.H. Ha, G. Kim, T. Shin, Visible-Light photocatalytic water splitting and norfloxacin degradation by reduced graphene oxide-coupled MnON nanospheres, ACS Appl. Energy Mater. 5 (2022) 12851–12859, https://doi.org/10.1021/acsaem.2c02455.

[32] K. Selvakumar, T.H. Oh, Y. Wang, T. Sadhasivam, S. Sadhasivam, M. Swaminathan, Fabrication of single tungsten/copper/cobalt atom oxide anchored $BiVO_4$-rGO for boosting photodegradation of norfloxacin and rhodamine B, J. Clean. Prod. 423 (2023), 138693, https://doi.org/10.1016/j.jclepro.2023.138693.

[33] X. Wang, S. Hu, H. Mao, X. Wei, S. Naraginti, Facile fabrication of $AgVO_3$/rGO/$BiVO_4$ hetero junction for efficient degradation and detoxification of norfloxacin, Environ. Res. 227 (2023), 115623, https://doi.org/10.1016/j.envres.2023.115623.

[34] K. Chakraborty, T. Pal, S. Ghosh, RGO-ZnTe: A graphene based composite for tetracycline degradation and their synergistic effect, ACS Appl. Nano Mater. 1 (2018) 3137–3144, https://doi.org/10.1021/acsanm.8b00295.

[35] K. Chakraborty, S. Ibrahim, P. Das, S. Ghosh, T. Pal, Solar light responsive photocatalytic activity of reduced graphene oxide–zinc selenide nanocomposite, J. Mater. Eng. Perform. 27 (2018) 2617–2621, https://doi.org/10.1007/s11665-017-3024-9.

[36] S. Bai, X. Shen, G. Zhu, A. Yuan, J. Zhang, Z. Ji, D. Qiu, The influence of wrinkling in reduced graphene oxide on their adsorption and catalytic properties, Carbon 60 (2013) 157–168, https://doi.org/10.1016/j.carbon.2013.04.009.

[37] Q. Zheng, B. Zhang, X. Lin, X. Shen, N. Yousefi, Z.-D. Huang, Z. Li, J.-K. Kim, Highly transparent and conducting ultralarge graphene oxide/single-walled carbon nanotube hybrid films produced by Langmuir–Blodgett assembly, J. Mater. Chem. 22 (2012) 25072–25082, https://doi.org/10.1039/C2JM34870E.

[38] G.T.S. How, A. Pandikumar, H.N. Ming, L.H. Ngee, Highly exposed 001 facets of titanium dioxide modified with reduced graphene oxide for dopamine sensing, Sci. Rep. 4 (2014) 05044, https://doi.org/10.1038/srep05044.

[39] W. Zhao, Y. Liu, Z. Wei, S. Yang, H. He, C. Sun, Fabrication of a novel p–n heterojunction photocatalyst n-$BiVO_4$@p-$MoS_2$ with core–shell structure and its excellent visible-light photocatalytic reduction and oxidation activities, Appl. Catal. B Environ. 185 (2016) 242–252, https://doi.org/10.1016/j.apcatb.2015.12.023.

[40] R. Yousefi, H.R. Azimi, M.R. Mahmoudian, Wan Jeffrey Basirun, The effect of defect emissions on enhancement photocatalytic performance of ZnSe QDs and ZnSe/rGO nanocomposites, Appl. Surf. Sci. 435 (2018) 886–893, https://doi.org/10.1016/j.apsusc.2017.11.183.

[41] H.Y. Hafeez, J. Mohammed, C.E. Ndikilar, A.B. Suleiman, R.S. Sa'id, I. Muhammad, Synergistic utilization of magnetic rGO/$NiFe_2O_4$-g-$C_3N_4$ S-Scheme heterostructure photocatalyst with enhanced charge carrier separation and transfer: A highly stable and robust photocatalyst for efficient solar fuel (hydrogen) generation, Ceram. Int. 49 (2023) 5269–5278, https://doi.org/10.1016/j.ceramint.2022.10.045.

[42] H. Kadkhodayan, T. Alizadeh, Fabrication of high-performance multifunctional Fe-doped $La_2ZnTiO_6$ double perovskite/activated carbon nanocomposite for efficient photocatalytic degradation of dyes, nitrate and carbon dioxide pollutants, Mater. Today Chem. 26 (2022), 101034, https://doi.org/10.1016/j.mtchem.2022.101034.

[43] T. Li, A. Abdelhaleem, W. Chu, W. Xu, Efficient activation of oxone by pyrite for the degradation of propanil: kinetics and degradation pathway, J. Hazard. Mater. 403 (2021), 123930, https://doi.org/10.1016/j.jhazmat.2020.123930.

[44] S. Kar, T. Pal, S. Ghosh, Removal of Norfloxacin from wastewater by adsorption onto $SnS_2$ followed by photocatalytic degradation, e202300878, ChemistrySelect 8 (2023), https://doi.org/10.1002/slct.202300878.

[45] Y. Li, T. Yang, S. Qiu, W. Lin, J. Yan, S. Fan, Q. Zhou, Uniform N-coordinated single-atomic iron sites dispersed in porous carbon framework to activate PMS for efficient BPA degradation via high-valent iron-oxo species, Chem. Eng. J. 389 (2020), 124382, https://doi.org/10.1016/j.cej.2020.124382.

[46] P. Chena, Y. Goua, J. Nib, Y. Lianga, B. Yangc, F. Jia, S. Song, Efficient ofloxacin degradation with Co(II)-doped $MoS_2$ nano-flowers as PMS activator under visible-light irradiation, Chem. Eng. J. 401 (2020), 125978, https://doi.org/10.1016/j.cej.2020.125978.

[47] P. Luo, W. Liu, D. Zhu, B. Sun, Y. Cao, Y. Wang, One-step synthesis of $Ti^{3+}$ self-doped CTO/rGO composites by pulsed laser ablation in liquid with enhanced photocatalytic activity in water purification, Colloids Surf. A Physicochem. Eng. Asp. 655 (2022), 130216, https://doi.org/10.1016/j.colsurfa.2022.130216.

[48] B. Xia, F. Deng, S. Zhang, L. Hua, X. Luo, M. Ao, Design and synthesis of robust Z-scheme ZnS-$SnS_2$ N-N heterojunctions for highly efficient degradation of pharmaceutical pollutants: Performance, valence/conduction band offset photocatalytic mechanisms and toxicity evaluation, J. Hazard. Mater. 392 (2020), 122345, https://doi.org/10.1016/j.jhazmat.2020.122345.

[49] Z. Yang, J. Yan, J. Lian, H. Xu, X. She, H. Li, g-$C_3N_4$/$TiO_2$ Nanocomposites for degradation of ciprofloxacin under visible light irradiation, ChemistrySelect 1 (2016) 5679–5685, https://doi.org/10.1002/slct.201600861.

[50] X. Bao, H. Li, Z. Wang, F. Tong, M. Liu, Z. Zheng, P. Wang, H. Cheng, Y. Liu, Y. Dai, Y. Fan, Z. Li, B. Huang, $TiO_2$/$Ti_3C_2$ as an efficient photocatalyst for selective oxidation of benzyl alcohol to benzaldehyde, Appl. Catal. B Environ. 286 (2021), 119885, https://doi.org/10.1016/j.apcatb.2021.119885.

[51] C. Zhang, M. Jia, Z. Xu, W. Xiong, Z. Yang, J. Cao, H. Peng, H. Xu, Y. Xiang, Y. Jing, Constructing 2D/2D N-ZnO/g-$C_3N_4$ S-scheme heterojunction: efficient photocatalytic performance for norfloxacin degradation, Chem. Eng. J. 430 (2022), 132652, https://doi.org/10.1016/j.cej.2021.132652.

[52] X. Lv, D.Y.S. Yan, F.L. –Y. Lam, Y.H. Ng, S. Yin, A.K. An, Solvothermal synthesis of copper-doped BiOBr microflowers with enhanced adsorption and visible-light driven photocatalytic degradation of norfloxacin, Chem. Eng. J. 401 (2020), 126012, https://doi.org/10.1016/j.cej.2020.126012.